Inorganic Chemistry

ARTICLE

pubs.acs.org/IC

Weak Interactions Modulating the Dimensionality in Supramolecular Architectures in Three New Nickel(II)-Hydrazone Complexes, Magnetostructural Correlation, and Catalytic Potential for Epoxidation of Alkenes under Phase Transfer Conditions

Dipali Sadhukhan,[†] Aurkie Ray,[†] Guillaume Pilet,[‡] Corrado Rizzoli,[§] Georgina M. Rosair,[∥] Carlos J. Gómez-García,[⊥] Sandra Signorella,[⊗] Sebastián Bellú,[⊗] and Samiran Mitra*[,†]

[†]Department of Chemistry, Jadavpur University, Raja S. C. Mullick Road, Kolkata 700032, West Bengal, India

[‡]Groupe de Crystallographie et IngénierieMoléculaireLaboratoire des Multimatériaux et Interfaces, UMR 5615 CNRS, Université Claude Bernard Lyon 1, Bât. Jules Raulin, 43 bd du 11 Novembre, 1918 69622 Villeurbanne, Cedex, France

[§]Dipartimento di Chimica Generale ed Inorganica, ChimicaAnalitica, Chimica Fisica, Universitá degli Studi di Parma, Viale G. P. Usberti 17/A I-43100 Parma, Italy

[∥]School of Engineering and Physical Sciences, Heriot Watt University, Edinburgh EH14 4AS, U.K.

[⊥]Instituto de Ciencia Molecular (ICMol), Universidad de Valencia, Parque Científico, 46980 Paterna, Spain

[⊗]Instituto de Química Rosario (IQUIR)−CONICET, Facultad de Ciencias Bioquímicas y Farmacéuticas, Universidad Nacional de Rosario, Suipacha 531, S2002LRK Rosario, Argentina

Supporting Information

ABSTRACT: Three different ONO donor acetyl hydrazone Schiff bases have been synthesized from the condensation of acetic hydrazide with three different carbonyl compounds: salicylaldehyde (HL^1), 2-hydroxyacetophenone (HL^2), and 2, 3-dihydroxybenzaldehyde (HL^3). These tridentate ligands are reacted with $Ni(OOCCF_3)_2 \cdot xH_2O$ to yield three new Ni(II) complexes having distorted octahedral geometry at each Ni center: $[Ni(L^1)(OOCCF_3)(CH_3OH)]_2$ (**1**), $[Ni(L^2)(OOCCF_3)(H_2O)]_2$ (**2**), and $[Ni(L^3)(L^3H)](OOCCF_3)(H_2O)_{1.65}(CH_3OH)_{0.35}$ (**3**). The ligands and the complexes have been characterized by elemental analysis and IR and UV−vis spectroscopy, and the structures of the complexes have been established by single crystal X-ray diffraction (XRD) study. **1** and **2** are centrosymmetric dinuclear complexes and are structural isomers whereas **3** is a *bis* chelated cationic monomer coordinated by one neutral and one monoanionic ligand. O−H···O hydrogen bonds in **3** lead to the formation of a dimer. Slight steric and electronic modifications in the ligand backbone provoke differences in the supramolecular architectures of the complexes, leading to a variety of one, two, and three-dimensional hydrogen bonded networks in complexes **1**−**3** respectively. Variable temperature magnetic susceptibility measurements reveal that moderate antiferromagnetic interactions operate between phenoxo bridged Ni(II) dimers in **1** and **2** whereas very weak antiferromagnetic exchange occurs through hydrogen bonding and $\pi-\pi$ stacking interactions in **3**. All complexes are proved to be efficient catalysts for the epoxidation of alkenes by NaOCl under phase transfer condition. The efficiency of alkene epoxidation is dramatically enhanced by lowering the pH, and the reactions are supposed to involve high valent Ni^{III}−OCl or Ni^{III}−O· intermediates. **3** is the best epoxidation catalyst among the three complexes with 99% conversion and very high turnover number (TON, 396).

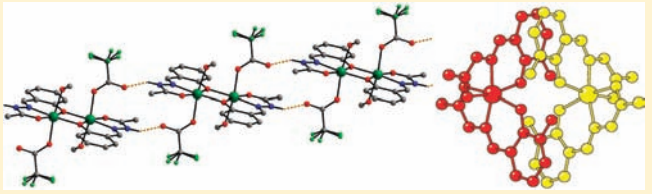

INTRODUCTION

Molecular self-assembly driven by weak interactions such as hydrogen-bonding, $\pi\cdots\pi$, C−H···π, van der Waals interactions, and so forth are currently of tremendous research interest in the fields of molecule based materials.[1,2] Among these weak interactions hydrogen-bonding is the strongest one with bond energies in the range 0.2−39 kcal mol^{-1},[3] while van der Waals interactions range around 1 kcal mol^{-1}.[4] The directional properties of the hydrogen-bonding interaction associates discrete molecules into aggregate structures that are sufficiently stable to be considered as independent chemical species. Chemistry can borrow nature's strategy to utilize hydrogen-bonding as well as other noncovalent interactions as found in secondary and tertiary structures of proteins such as the double helix folding of DNA, hydrophobic self-organization of phospholipids in cell membrane, and so forth.[5] In supramolecular chemistry hydrogen-bonding plays an important role in forming a variety of architectures.[1a,6,7] Thus, the wise modulation and tuning of the complementary sites responsible for hydrogen-bond formation

Received: April 24, 2011
Published: July 28, 2011

have led to its application in supramolecular electronics,[8] host–guest chemistry,[9] self-assembly of molecular capsules,[10] nanotubes,[11] and so forth. The molecular aggregates formed by a variety of hydrogen-bonding patterns can be systematically analyzed by applying graph set theory developed by Etter and co-workers.[12] Complex networks can be recognized and reduced to combination of four simple patterns, each specified by a designator: chains (C), rings (R), intramolecular hydrogen-bonded patterns (S), and other finite patterns (D).

Transition metal complexes derived from hydrazone Schiff bases can form diverse supramolecular networks as reported previously by various research groups[13] as well as by us.[14] Albeit, most of these works are based on aryl-hydrazone ligands, and there are very few reports of metal complexes of hydrazone-Schiff bases derived from alkyl hydrazides;[14c,d,i,15] to the best of our knowledge, no structural report of Ni(II) complexes of acetyl hydrazones with extensive supramolecular interactions has been published so far.

Octahedral Ni(II) Schiff base complexes possess magnetic interactions covering a broad range, from antiferromagnetism to ferromagnetism.[16] Moreover, interest in epoxidation of alkenes catalyzed by transition metal complexes is growing because of the increased use of epoxides in agro- and pharmacological chemistry.[17] Although historically Mn(salen) complexes[18] were considered as important candidates for epoxidation of alkenes, recently some mono and dinuclear Ni(II) Schiff base/macrocyclic complexes have been shown to be used for this purpose.[19,20] The catalytic efficiency of Ni(II) complexes depends on the nature of terminal oxidants as well as on the specific ligand environment.

In the present work, we have synthesized three new ONO donor hydrazone ligands from the condensation of acetic hydrazide with three different carbonyl compounds, namely, salicylaldehyde (HL^1), 2-hydroxyacetophenone (HL^2), and 2,3-dihydroxybenzaldehyde (HL^3) (Scheme 1). We have also prepared and characterized the three reaction products of these ligands with $Ni(OOCCF_3)_2 \cdot xH_2O$. These three products are formed by distorted octahedral Ni(II) complexes, formulated as $[Ni(L^1)(OOCCF_3)(CH_3OH)]_2$ (**1**), $[Ni(L^2)(OOCCF_3)(H_2O)]_2$ (**2**), and $[Ni(L^3)(L^3H)](OOCCF_3)(H_2O)_{1.65}(CH_3OH)_{0.35}$ (**3**). Interestingly, the three complexes show one-, two-, and three-dimensional (1D, 2D, 3D) H-bonded networks, in **1**, **2**, and **3**, respectively. The magnetic measurements show the presence of an intramolecular moderate antiferromagnetic coupling in **1** and **2**, and a weak intermolecular antiferromagnetic interaction in **3** via O–H···O hydrogen bonding and $\pi-\pi$ stacking. We have also evaluated the ability of the Ni(II)-hydrazone complexes to catalyze the epoxidation of various alkenes using NaClO under phase transfer conditions. The pH dependence of the ClO^- based alkene epoxidation reactions shows dramatic rate acceleration at low pH. Two probable mechanistic pathways have also been proposed for the catalytic reactions.

EXPERIMENTAL SECTION

Materials. All solvents were of reagent grade and used without further purification. Acetic hydrazide, salicylaldehyde, 2-hydroxyacetophenone, and 2,3-dihydroxybenzaldehyde were purchased from Aldrich Chemical Co. and used as received. Nickel trifluoroacetate was prepared by treatment of nickel carbonate (E. Merck, India) with 60% trifluoroacetic acid (E. Merck, India) followed by slow evaporation on a steam bath. It was then filtered through a fine glass-frit and preserved in a $CaCl_2$ desiccator for further use. *cis*-Stylbene, cyclohexene, *trans*-4-octene, styrene, and benzyltributylammonium chloride, used in the catalytic experiments, were from Aldrich and used as received. Chloroform was of HPLC grade (Merk). Commercial bleach was used as the NaClO source.

Scheme 1. Scheme of Syntheses of the Ligands: HL^1, HL^2, and HL^3

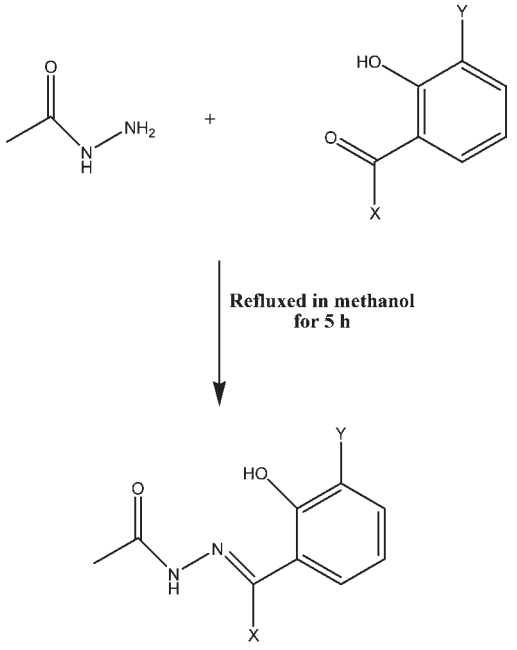

L^1H: X= H, Y= H
L^2H: X= CH_3, Y= H
L^3H: X= H, Y= OH

Syntheses of the Hydrazone Ligands [L^1H, L^2H, L^3H]. The ligand L^1H [(*E*)-*N*′-(2-hydroxybenzylidene)acetohydrazide] was prepared by the condensation of acetic hydrazide (0.74 g, 10 mmol) with salicylaldehyde (1.221 g, 10 mmol) in presence of a single drop of glacial acetic acid in methanol medium (200 mL). On refluxing the methanolic solution for 5 h a colorless solution was obtained. The solvent was removed under reduced pressure, and the white residue was purified by recrystallization to obtain colorless shiny crystals. Yield 1.55 g (87%). Anal. Calcd. (%) for $C_9H_{10}N_2O_2$ (M = 178.1 g/mol): C, 60.66; H, 5.66; N, 15.72. Found: C, 60.58; H, 5.78; N, 15.69. FT-IR bands (KBr, cm^{-1}): ν(C=N) 1623, ν(C=O) 1684.

The ligand L^2H [(*E*)-*N*′-(1-(2-hydroxyphenyl)ethylidene)acetohydrazide] was prepared by the condensation of 200 mL of a methanolic solution of acetic hydrazide (0.74 g, 10 mmol) with 2-hydroxyacetophenone (1.362 g, 10 mmol) following the same procedure as for L^1H. In this case also shiny colorless crystals were obtained. Yield 1.77 g (92%). Anal. Calcd. (%) for $C_{10}H_{12}N_2O_2$ (M = 192.1 g/mol): C, 62.49; H, 6.29; N, 14.57. Found: C, 62.58; H, 6.23; N, 14.49. FT-IR bands (KBr, cm^{-1}): ν(C=N) 1606, ν(C=O) 1667.

The ligand L^3H [(*E*)-*N*′-(2,3-dihydroxybenzylidene)acetohydrazide] was prepared by the condensation of 200 mL of a methanolic solution of acetic hydrazide (0.74 g, 10 mmol) with 2,3-dihydroxybenzaldehyde (1.381 g, 10 mmol) in the presence of a single drop of glacial acetic acid to form a light yellow solution obtained on 5 h reflux. After removing the solvent under reduced pressure a light yellow solid was obtained. This solid was recrystallized to obtain light yellow crystals of L^3H. Yield 1.61 g (83%). Anal. Calcd. (%) for $C_9H_{10}N_2O_3$ (M = 194.1 g/mol): C, 55.67; H, 5.19; N, 14.43. Found: C, 55.68; H, 5.08; N, 14.49. FT-IR bands (KBr, cm^{-1}): ν(C=N) 1614, ν(C=O) 1664.

dx.doi.org/10.1021/ic200846j |*Inorg. Chem.* 2011, 50, 8326–8339

Synthesis of $[Ni(L^1)(OOCCF_3)(CH_3OH)]_2$ (1). $Ni(OOCCF_3)_2 \cdot xH_2O$ (0.213 g, 0.75 mmol) was dissolved in 20 mL of a 1:1 v/v mixture of methanol and acetonitrile. Ten milliliters of a methanolic solution of the Schiff base L^1H (0.089 g, 0.5 mmol) was added to the former followed by one drop of triethylamine, and it was heated to 60 °C with stirring for 30 min. The bright green solution was kept in a refrigerator at 16 °C. Green cubic single crystals suitable for X-ray diffraction were obtained within 2 days. Crystals were isolated by filtration and were air-dried. Yield: 0.65 g (85%). Anal. Calcd. for $C_{24}H_{26}F_6N_4Ni_2O_{10}$ (M = 761.90 g/mol): C, 37.80; H, 3.41; N, 7.35. Found: C, 37.69; H, 3.60; N, 7.38%. FT-IR bands (KBr, cm^{-1}): ν(O−H) 3431, ν(C═N) 1547, ν(C═O) 1607, ν_{asym}-(COO^-) 1676, $\nu_{sym}(COO^-)$ 1385, ν(C−F) 1201, ν(Ni−N) 462. UV−vis bands (CH_3CN, nm): LMCT 375, n→π^* 284, π→π^* 240.

Synthesis of $[Ni(L^2)(OOCCF_3)(H_2O)]_2$ (2). $Ni(OOCCF_3)_2 \cdot xH_2O$ (0.213 g, 0.75 mmol) was dissolved in 10 mL of 2-propanol. Ten milliliters of a methanolic solution of the Schiff base L^2H (0.096 g, 0.5 mmol) was added to the former. One drop of triethylamine was added into the mixture, and it was heated to 60 °C with stirring for 30 min. The bright green solution was kept at room temperature for slow evaporation of solvent. Green block shaped single crystals suitable for X-ray diffraction were obtained after 3 days. Crystals were isolated by filtration and were air-dried. Yield: 0.62 g (82%). Anal. Calcd. for $C_{24}H_{26}F_6N_4Ni_2O_{10}$ (M = 761.90 g/mol): C, 37.80; H, 3.41; N, 7.35. Found: C, 37.75; H, 3.46; N, 7.47%. FT-IR bands (KBr, cm^{-1}): ν(O−H) 3410, ν(C═N) 1542, ν(C═O) 1596, $\nu_{asym}(COO^-)$ 1680, $\nu_{sym}(COO^-)$ 1376, ν(C−F) 1199, ν(Ni−N) 445. UV−vis bands (CH_3CN, nm): LMCT 344, n→π^* 275, π→π^* 240.

Synthesis of $[Ni(L^3)(L^3H)](OOCCF_3)(H_2O)_{1.65}(CH_3OH)_{0.35}$ (3). $Ni(OOCCF_3)_2 \cdot xH_2O$ (0.213 g, 0.75 mmol) was dissolved in 10 mL of acetonitrile. Ten milliliters of a methanolic solution of the Schiff base L^3H (0.097 g, 0.5 mmol) was added to the former. One drop of triethylamine was added into the mixture, and it was heated to 60 °C with stirring for 45 min. The bright green solution was kept in refrigerator at 16 °C. Green block shaped single crystals suitable for X-ray diffraction were obtained after 3 days. Crystals were isolated by filtration and were air-dried. Yield: 0.47 g (79%). Anal. Calc. for $C_{20.35}H_{23.7}N_4NiF_3O_{10}$ (M = 600.02 g/mol): C, 40.70; H, 3.95; N, 9.33. Found: C, 40.59; H, 3.80; N, 9.28%. FT-IR bands (KBr, cm^{-1}): ν(O−H) 3321, ν(C═N) 1576, ν(C═O) 1611, $\nu_{asym}(COO^-)$ 1671, $\nu_{sym}(COO^-)$ 1387, ν(C−F) 1191, ν(Ni−N) 472 cm^{-1}. UV−vis bands (CH_3CN, nm): LMCT 389, n→π^* 299, π→π^* 240.

Physical Measurements. The Fourier Transform Infrared spectra were recorded in the range 4000−400 cm^{-1} on a Perkin-Elmer RX I FT-IR spectrophotometer with solid KBr pellets. The electronic spectra in HPLC grade acetonitrile were recorded at 300 K on a Perkin−Elmer Lambda 40 (UV−Vis) spectrometer in a 1 cm quartz cuvette in the range 200−800 nm. C, H, and N microanalyses were carried out with a Perkin-Elmer 2400 II elemental analyzer. The positive ion ESI-MS was performed in a QTOF micro mass spectrometer. The magnetic susceptibility measurements were carried out in the temperature range 2−300 K with an applied magnetic field of 0.1 T on polycrystalline samples of compounds **1**−**3** (with masses of 28.04, 33.75, and 21.12 mg, respectively) with a Quantum Design MPMS-XL-5 SQUID susceptometer. The isothermal magnetizations were performed on the same samples at 2 K with magnetic fields up to 8 T in a Quantum Design PPMS-9 equipment for **1** and **2** and up to 5 T in the SQUID susceptometer for **3**. The susceptibility data were corrected for the sample holder using the same conditions and for the diamagnetic contributions of the salt as deduced by using tables of Pascal's constants (χ_{dia} = -343.6×10^{-6}, -314.3×10^{-6}, and -332.0×10^{-6} emu.mol^{-1} for **1**−**3**, respectively). HPLC experiments were performed with a Varian ProStar chromatograph equipped with DAD 335 detector using a Varian Microsorb-MV 100-5 C18 column (250 × 4.6 × 1/4″), with a Zeltec thermostatted heater. Samples were eluted with a 70:30 acetonitrile/methanol mixture at a flow rate of 0.4 mL/min at 40 °C. Under these experimental conditions, retention times (R_t) were styrene (R_t = 7.88 min), styrene epoxide (R_t = 7.17 min), benzaldehyde (R_t = 7.05 min), *cis*-stylbene (R_t = 8.51 min), cyclohexene (R_t = 9.47 min), cyclohexene oxide (R_t = 7.13), and *trans*-4-octene (R_t = 11.39 min). Calibration curves of authentic alkene and product samples were used to quantify the alkene conversion and product selectivity. At least two independent experiments were performed for each set of reaction conditions. Blank experiments with the oxidant and using the same experimental conditions except catalyst were performed. Alkene conversion in absence of the complex was 0−5%.

Crystal Data Collection and Refinement. Intensity data were collected using MoKα radiation with a Nonius Kappa CCD diffractometer at 293 K for **1**, on a Bruker X8 APEXII diffractometer at 100 K for **2**, and on a Bruker SMART 1000 CCD diffractometer at 294 K for **3**. Data collections were performed with the COLLECT,[21] APEX 2,[22] and SMART[23] programs for **1**, **2**, and **3**, respectively. Programs DENZO/SCALEPACK,[24] SAINT,[25] and SMART[23] were used for data reduction of **1**, **2**, and **3**, respectively. Empirical absorption corrections were carried out by multiscan technique using DENZO/SCALEPACK for **1** and SADABS[26] for **2** and **3**. The structures were solved by direct methods using the SIR97[27] program for **1** and **3**, and the SHELXS-97[28] program for **2**. All structures were refined by full-matrix least-squares methods with the program CRYSTALS[29] for **1** or SHELXL-97[28] for **2** and **3**. In **1**, the F atoms of the trifluoroacetate anions are disordered over two orientations, with site occupancy factors of 0.6 and 0.4. All H atoms of **1** and **2** and most C-bound H atoms of **3** were generated geometrically and were included in the refinement in the riding model approximation. In **3**, the water molecule including the O9 atom was found to be disordered over two positions with site occupancy factors of 0.65 and 0.35. The displacement parameters of the disordered oxygen atom were restrained to be the same. A second water molecule (atom O10A) and a methanol molecule (atoms O10B and C21) were found to occupy the same site, and were refined with site occupancy factors of 0.65 and 0.35 for the water and methanol molecule, respectively. During the refinement, the C−O bond was constrained to 1.40(1) Å. The water molecule H atoms were located in a difference Fourier map and placed at chemically sensible positions, and refined with the O···H and H···H distances constrained to 0.86(1) and 1.36(2) Å, respectively, and with U_{iso}(H) = 1.5U_{eq}(O). The H atoms of the methanol molecule were calculated geometrically and refined as riding, with O−H = 0.86 Å, C−H = 0.96 Å, and with U_{iso}(H) = 1.5U_{eq}(C, O). The ligand hydroxy H atoms were located in a difference Fourier map and refined using the riding model approximation, with O−H = 0.86 Å. Selected crystallographic data, experimental conditions, and relevant features of the structural refinements for all the complexes are summarized in Table 1.

Catalysis Experiments. Ten micromol of catalyst (7.6 mg of **1**, 7.9 mg of **2** or 6.0 mg of **3**), 10 μmol of phase transfer catalyst benzyltributylammonium chloride (3 mg), and 0.4 mmol of alkene (41 μL cyclohexene, 63 μL of *trans*-4-octene, 71 μL of *cis*-stylbene or 46 μL styrene), were suspended in 2 mL of freshly distilled Cl_3CH. With stirring and at a controlled temperature of 20 °C, 2 mL of an aqueous solution of 0.7 M NaClO were added. In experiments at pH 9−11, the aqueous layer was prepared beforehand, buffered with $Na_2B_4O_7$ and adjusted to the desired pH with either 4 N NaOH or concentrated HCl. In a series of experiments at pH 9, 1 μmol of catalyst was used. The reaction was stirred at constant temperature, and the reaction time for maximal conversion was determined by withdrawing periodically aliquots of 20 μL from the Cl_3CH layer that were subjected to HPLC analysis. This time was used to monitor the efficiency of the catalyst. Aliquots were diluted with 2 mL of acetonitrile and filtered through a 0.2 μm membrane prior to injection into the chromatograph. In every case, the epoxide was the only reaction product.

RESULTS AND DISCUSSIONS

Crystal Structures of $[Ni(L^1)(OOCCF_3)(CH_3OH)]_2$ (1) and $[Ni(L^2)(OOCCF_3)(H_2O)]_2$ (2). The asymmetric units of **1** and **2**

Table 1. Crystal Structure Parameters of 1, 2, and 3

	1	2	3
empirical formula	$C_{24}H_{26}F_6N_4Ni_2O_{10}$	$C_{24}H_{26}F_6N_4Ni_2O_{10}$	$C_{20.35}H_{23.7}N_4NiF_3O_{10}$
formula weight (g mol^{-1})	761.90	761.90	600.02
temperature	293 K	100 K	294 K
wavelength	0.71069 Å	0.71073 Å	0.71071 Å
crystal system	triclinic	triclinic	monoclinic
space group	$P\bar{1}$ (No. 2)	$P\bar{1}$ (No. 2)	$C2/c$ (No. 15)
a (Å)	9.169(5)	7.210(4)	17.7819(10)
b (Å)	9.388(5)	10.186(8)	18.5529(11)
c (Å)	10.615(5)	10.376(6)	15.248(9)
α (deg)	114.555(5)	77.13(2)	90
β (deg)	106.173(5)	73.77(2)	95.7711(10)
γ (deg)	96.843(5)	82.21(3)	90
V (Å^3)	768.8(7)	711.1(8)	5005(3)
Z	1	1	8
d_{calc} (g cm^{-3})	1.646	1.779	1.593
μ (mm^{-1})	1.279	1.427	0.859
F(000)	388	388	2470
crystal size (mm^3)	0.08 × 0.09 × 0.11	0.14 × 0.34 × 0.42	0.11 × 0.15 × 0.21
θ range (deg)	2.6−29.4	2.1−26.4	1.6−25.5
reflections collected	6005	4846	24822
ind. reflections	3522	2447	4687
R(int)	0.020	0.038	0.037
reflections used	2566	1817	4687
parameters refined	199	208	390
goodness-of-fit on F^2	1.13	1.18	1.00
final R indices	R = 0.0573	$R1$ = 0.0437	R = 0.0353
	wR = 0.0631	$wR2$ = 0.0840	wR = 0.0934
	[$I > 3\sigma(I)$]	[$I > 2\sigma(I)$]	[$I > 2\sigma(I)$]
$\Delta\rho_{max}$ and $\Delta\rho_{min}$	1.16 and −1.21 e Å^{-3}	0.87 and −0.83 e Å^{-3}	0.44 and −0.34 e Å^{-3}

belong to the same space group ($P\bar{1}$), and, interestingly, they have the same molecular formula, that is, the same number of atoms of the same elements, connected together in different ways; hence, **1** and **2** are structural isomers. It is to be noted that this isomerism arises from the presence of different ligands whose total empirical formula is the same, but they present different connectivity; therefore, they are structural isomers, although they can not be classified as coordination nor ionization nor linkage isomers.

The asymmetric units of the Ni(II) complexes **1** and **2** are depicted in Figures 1a and 1b, respectively, and selected bond lengths and angles are listed in Table 2. Both complexes are positioned over centers of inversion generating bis(μ-phenoxo) bridged dinuclear structures where each six coordinate Ni(II) ion can be defined as distorted $NiNO_5$ octahedra (Figure 2). The ONO donor Schiff base ligands occupy three of the equatorial sites with the fourth site occupied by the bridging phenoxo oxygen atom. One of the axial positions is occupied by the oxygen atom (O21) of a terminally coordinated trifluoroacetate anion in both complexes whereas the second axial position is occupied by an oxygen atom (O31) belonging to a methanol molecule in **1** and to a water molecule in **2**. In both complexes the Ni1 atom is located slightly above the equatorial plane with a small out of plane deviation (0.050 Å in **1** and 0.036 Å in **2**) toward the axial O21 atom of the CF_3COO^- anion. The ONO donor ligands form effectively planar five and six membered chelate rings around the metal centers (Figure 2). The phenoxo oxygens (O1) form centrosymmetric double μ-phenoxo bridges between the two Ni atoms with Ni−O−Ni bond angles of 98.74(12)° and 99.06(15)° in **1** and **2**, respectively (Table 2). The twelve *cis* angles subtended at the metal center by adjacent N/O donor atoms vary in the range 78.8(1)−98.1(1)° in **1** and between 79.20(14)−98.07(13)° in **2** whereas the three *trans* angles are in the range 167.5(1)−171.01(13)° in both complexes. The deviation of the *cis* and *trans* bond angles subtended at the metal centers from the ideal values (Table 2) may be attributed to crystal packing forces, such as hydrogen-bonding observed in the structures and also to the inherent geometrical constraints of the ligands. The intramolecular Ni···Ni distances [3.077 and 3.066 Å in **1** and **2**, respectively] are similar to those observed in other double phenoxo bridged dinuclear nickel systems.[30,31]

The crystal packing of both complexes shows several intra- and intermolecular O−H···O, N−H···O, and C−H···O H-bonds shown in Figure 2 (a and b for **1** and **2**, respectively) and listed in Table 3. **1** presents rotational disorder of the F atoms of the coordinated CF_3COO^- anion, which are rotated over two sets of sites by about 40° along the C−C bond. In contrast, **2** does not show this disorder probably because of the stabilizing effect of the intramolecular O31−H15···F26 interaction, which is absent in **1**.

In **1** and **2** adjacent dimers are linked via pairs of N10−H23···O23 intermolecular H-bonds to form a 1D supramolecular

dx.doi.org/10.1021/ic200846j |*Inorg. Chem.* 2011, 50, 8326–8339

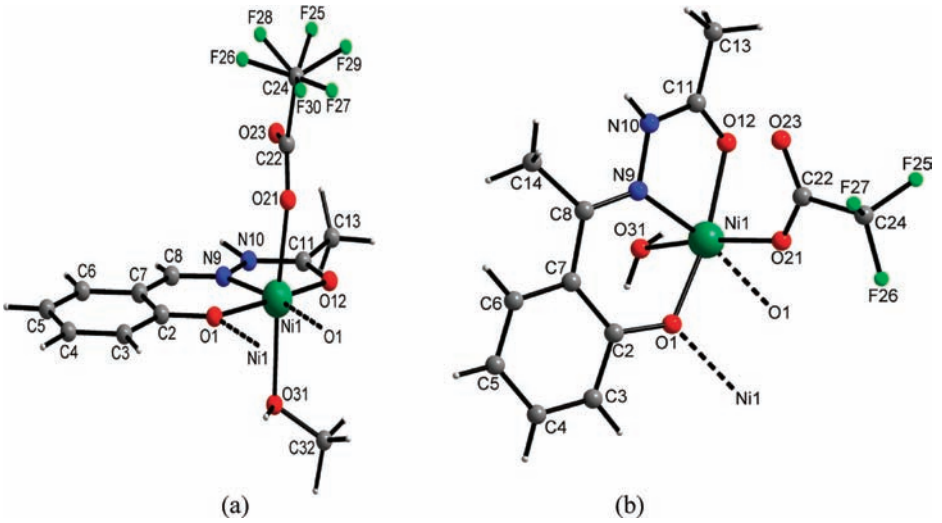

Figure 1. Perspective view of the asymmetric unit of **1** (a) and **2** (b). H atoms are shown as spheres of arbitrary radius.

Table 2. Selected Bond Lengths (Å) and Angles (deg) for 1 and 2

	1	2
	Bond Lengths (Å)	
Ni1−O1	2.012(3)	1.969(3)
Ni1−O1_a[a]	2.042(3)	2.064(3)
Ni1−N9	1.998(3)	2.015(4)
Ni1−O12	2.094(3)	2.083(4)
Ni1−O21	2.075(4)	2.083(3)
Ni1−O31	2.114(4)	2.094(3)
	Bond Angles (deg)	
O1−Ni1−O1_a[a]	81.3(1)	81.08(13)
O1−Ni1−N9	89.9(1)	89.6(0)
O1_a−Ni1−N9[a]	170.2(1)	170.41(14)
O1−Ni1−O12	167.5(1)	168.71(13)
O1_a−Ni1−O12[a]	110.7(1)	110.05(13)
N9−Ni1−O12	78.8(1)	79.20(14)
O1−Ni1−O21	92.0(1)	90.43(13)
O1_a−Ni1−O21[a]	84.1(1)	84.32(12)
N9−Ni1−O21	98.1(2)	98.07(13)
O12−Ni1−O21	92.8(2)	92.57(13)
O1−Ni1−O31	86.6(1)	88.44(13)
O1_a−Ni1−O31[a]	85.7(1)	86.69(12)
N9−Ni1−O31	92.0(2)	90.84(13)
O12−Ni1−O31	90.7(2)	90.25(13)
O21−Ni1−O31	169.8(1)	171.01(13)
Ni1−O1−Ni1_a[a]	98.7(1)	98.92(14)

[a] Symmetry transformations used to generate equivalent atoms: _a: $-x+1,-y+2,-z+2$.

self-assembly running parallel to the crystallographic *c* axis (Figures 3 and 4). The repeating motif of this intermolecular hydrogen-bond occurs in the form of a ring around an inversion center and is best described by the basic unitary graph set $R_2^2(14)$.[12] Besides these H-bonds, in **2** additional pairs of O31−H4···O12 interactions along the crystallographic *a* axis (Figure 4) link centrosymmetrically related molecules to form rings of graph set $R_2^2(8)$ into a 2D supramolecular architecture in the *ac* plane.

Structure of $[Ni(L^3)(L^3H)](OOCCF_3)(H_2O)_{1.65}(CH_3OH)_{0.35}$ (3). The asymmetric unit of **3** is shown in Figure 5, and the selected bond distances and angles are listed in Table 4. The Ni(II) ion displays a distorted octahedral coordination geometry with two Schiff base ligands coordinated to the Ni(II) ion as tridentate ONO chelating agents via the phenolic oxygen (O1 and O4), the azomethine nitrogen (N1 and N3), and the *keto* oxygen atoms (O3 and O6). The phenolic oxygen (O4) of one of the two Schiff bases coordinating the Ni(II) ion undergoes deprotonation during complexation and behaves as a mononegative ligand $(L^3)^-$, but the other one (O1) is protonated and behaves as a neutral ligand (L^3H). Therefore, the complex is monocationic and is stabilized by a trifluoroacetate counteranion in the lattice. The ligands are coordinated to the metal center with their coordinating atoms in a *meridional* configuration, being the phenolic (O1 and O4) and *keto* (O3 and O6) oxygen atoms in *cis* orientation to each-other and the azomethine nitrogen atoms (N1 and N3) in *trans* orientation (Figure 5). The 12 *cis* angles and the three *trans* angles subtended at the metal center show deviations from the ideal values (Table 4) that may be attributed to the restricted bite angles imposed by the planar tridentate Schiff bases. The equatorial plane of the NiN_2O_4 chromophore is defined by two phenolic (O1 and O4) and two ketonic (O3 and O6) oxygen atoms, while the two axial sites are occupied by the two azomethine nitrogen atoms (N1 and N3). The Ni−N (azomethine) bond distance is comparable with other bis chelated Ni(II) complexes of ONO and NNO donor Schiff base ligands.[32,33] The two ligands [L^3H and $(L^3)^-$] are almost orthogonal [the angle between the planes of the ONO donor sets is 88.24(4)°]. Generally in bis-chelated octahedral complexes containing two tridentate ONO or NNO donor ligands, the two coordinated ligands are identical and present the same charge.[32,34,35] Interestingly, in **3** one of the Schiff base ligands is protonated and appears as a neutral (L^3H) entity whereas the other one is deprotonated and appears as an anionic $(L^3)^-$ ligand. Such behavior of an ONO donor tridentate Schiff base in a bis-chelated Ni(II) complex is rather unusual.[33]

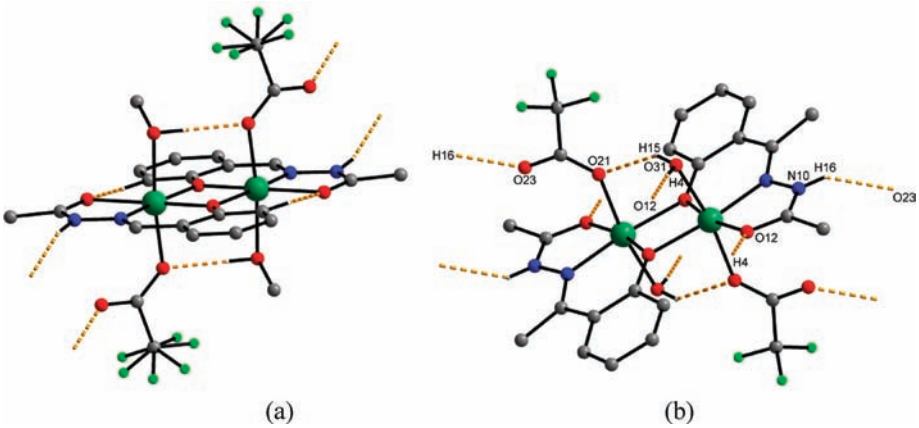

Figure 2. View of the centrosymmetric dimers in **1** (a) and **2** (b). Intra- and intermolecular hydrogen bonds are indicated by dashed lines.

Table 3. Hydrogen Bonding Interactions in 1 and 2

complex	D−H···A	d(D−H) Å	d(H···A) Å	d(D···A) Å	∠(D−H···A) deg
1	C3−H72···O12	1.00	2.34	3.272(9)	155
	O31−H1···O21	0.90	1.91	2.806(9)	179
	N10−H23···O23	0.99	1.83	2.765(9)	157
2	C3−H31···O12	0.93	2.34	3.232(6)	160
	C14−H141···N10	0.97	2.35	2.707(7)	101
	O31−H15···O21	0.81	2.13	2.828(5)	144
	O31−H15···F26	0.81	2.48	3.102(5)	135
	N10−H16···O23	0.85	2.07	2.809(5)	145
	O31−H4···O12	0.83	2.00	2.830(5)	172

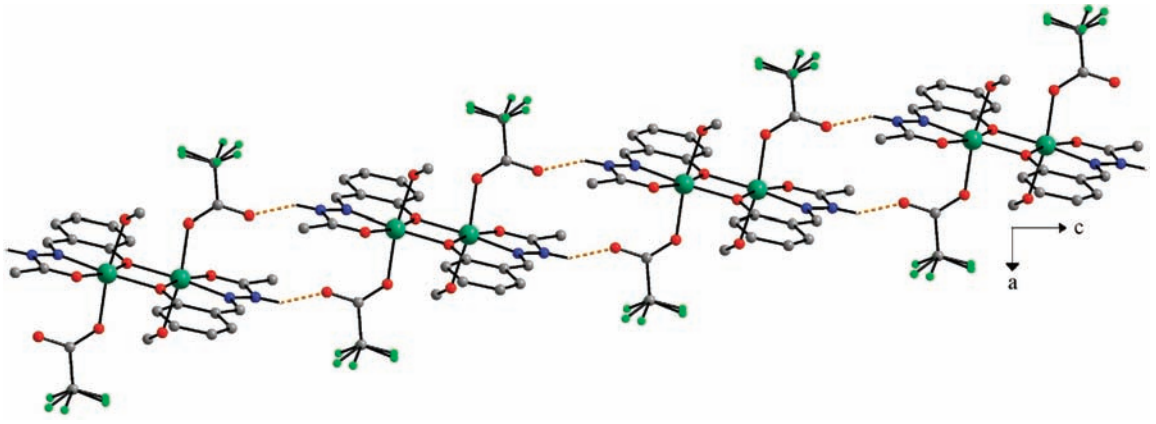

Figure 3. Packing diagram of **1** showing the 1D H-bonded network. The six possible positions of the 3 F atoms are indicated. Hydrogen atoms not involved in H-bonding are omitted for clarity.

The phenolic oxygen atoms (O1 and O2) of the protonated neutral ligand of one asymmetric unit act as hydrogen bond donors to the phenoxo oxygen atoms (O4 and O5) of the deprotonated anionic ligand of an adjacent unit (generated by the symmetry operation $1-x, y, 1/2-z$), forming a dimer via two pairs of cooperative O1−H10···O4^{i} and O2−H20···O5^{i} hydrogen bonds (Figure 6 and Table 5). This disposition is favored by the formation of two close $\pi-\pi$ stacking interactions between the aromatic rings of the symmetry related units belonging to the hydrogen bonded dimer (Figure 6). The interplanar average distance between the C1···C6 rings is 3.259 Å whereas that between the C10···C15 ones is 3.356 Å.

A further insight to the structure of **3** reveals the presence of several O−H···O, N−H···O, and C−H···O intermolecular H-bonding interactions (Table 5 and Figures 7a and 7b, where O10A and O10B, which alternatively occupy the same site of the lattice, are shown separately).

Note that although one of the two solvent molecules presents a disorder between a water and a methanol molecule, the formation of the three-dimensional network of H-bonds is

dx.doi.org/10.1021/ic200846j |*Inorg. Chem.* 2011, 50, 8326–8339

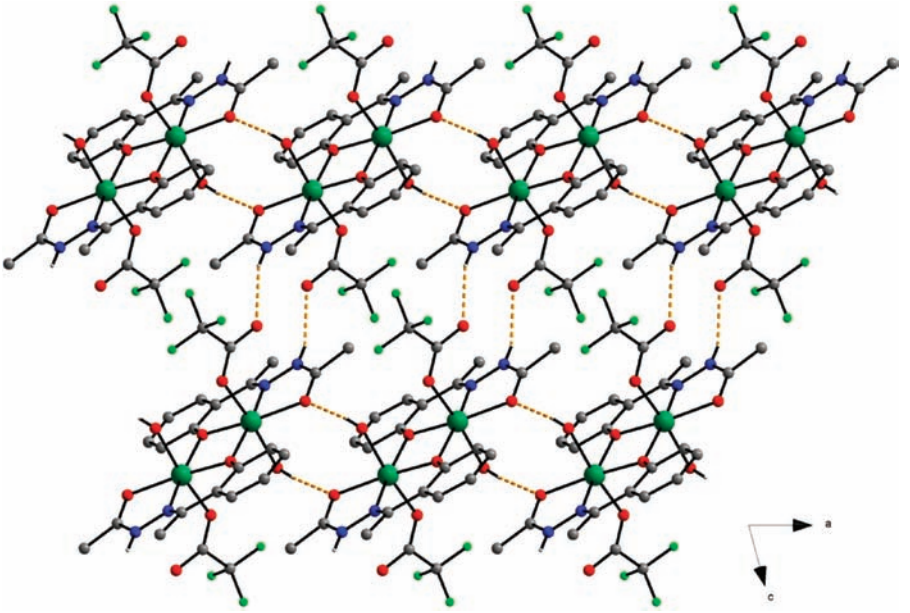

Figure 4. Packing diagram of **2** showing the 2D H-bonded network. Hydrogen atoms not involved in H-bonding are omitted for clarity.

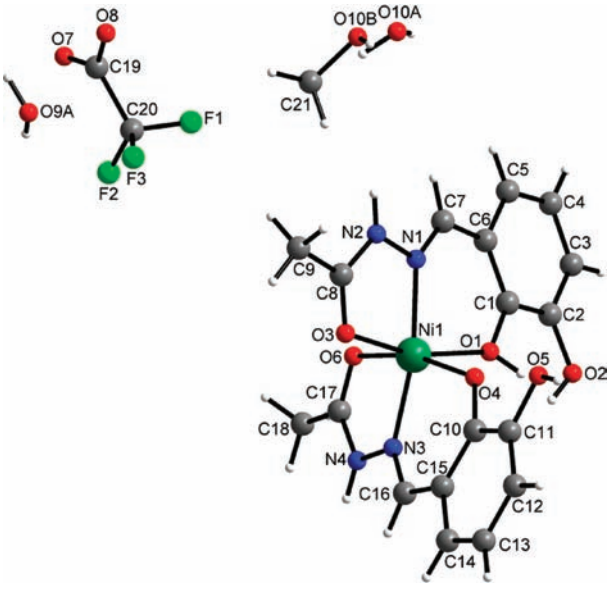

Figure 5. Asymmetric unit of **3** showing the disordered water (O10A) and methanol molecules (C21−O10B).

observed in both cases (Figure 8), the only difference being the stronger H-bond observed when the solvent is a water molecule compared to the methanol one. This may explain the higher occupancy factor of the water molecule compared to the methanol one.

Structural Comparison of the Three Complexes. A comparative study of the synthetic and structural aspects of the three complexes (**1**−**3**) reveals that the three Schiff base ligands (L^1H, L^2H, and L^3H) contain the same amine fragment, (acetic-hydrazide) but different carbonyl functions (salicylaldehyde, 2-hydroxyacetophenone, and 2,3-dihydroxybenzaldehyde) in L^1H, L^2H, and L^3H, respectively (Scheme 1), that is, we have modified the design of salicylaldehyde of L^1H by introducing a methyl group in the side chain in L^2H and an extra hydroxyl group in the aromatic ring in L^3H. Interestingly, these small modifications have led to important structural changes. When comparing the asymmetric units of **1** and **2**, we can see that the change of an H atom (in L^1H) by a $-CH_3$ group (in L^2H) implies a higher steric hindrance in **2** that precludes the coordination of the CH_3OH molecule, in contrast to **1**. These

Table 4. Selected Bond Lengths (Å) and Bond Angles (deg) for 3

Bond Lengths (Å)	
Ni1−O1	2.052(2)
Ni1−O3	2.089(2)
Ni1−O4	2.046(2)
Ni1−O6	2.067(2)
Ni1−N1	2.003(2)
Ni1−N3	2.002(2)
Bond Angles (deg)	
O1−Ni1−O3	163.97(7)
O1−Ni1−O4	88.74(6)
O1−Ni1−O6	89.03(7)
O1−Ni1−N1	87.07(7)
O1−Ni1−N3	99.34(7)
O3−Ni1−O4	87.95(7)
O3−Ni1−O6	97.88(7)
O3−Ni1−N1	78.29(8)
O3−Ni1−N3	96.18(8)
O4−Ni1−O6	165.79(7)
O4−Ni1−N1	101.98(7)
O4−Ni1−N3	87.50(7)
O6−Ni1−N1	91.92(8)
O6−Ni1−N3	79.02(8)
N1−Ni1−N3	168.73(8)

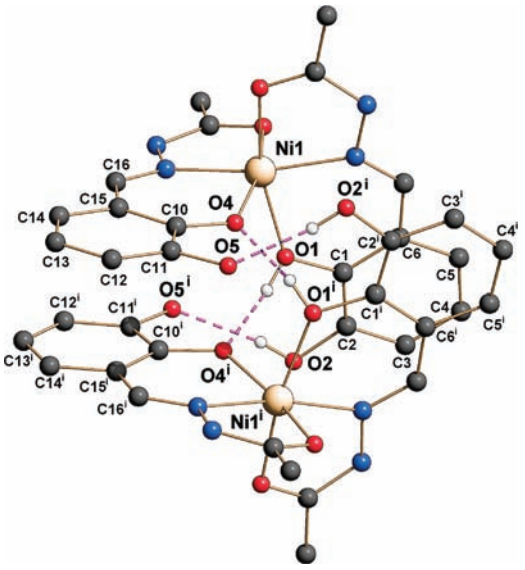

Figure 6. Dimeric unit formed by intermolecular O−H···O interaction in **3**. Hydrogen atoms not involved in hydrogen bonding are omitted for clarity (symmetry code: (i) $1-x, y, 1/2-z$). $\pi-\pi$ interactions are also prominent within the dimer.

Table 5. Hydrogen Bonding Interactions in 3[a]

D−H···A	d(D−H) Å	d(H···A) Å	d(D···A) Å	∠(D−H···A) deg
O1−H10···O4^{i}	0.82	1.66	2.474(2)	171
O2−H20···O5^{i}	0.82	1.95	2.754(3)	165
O5−H50···O8^{i}	0.82	1.88	2.684(3)	165
C4−H4···O8^{iv}	0.93	2.52	3.391(4)	157
C14−H14···O3^{ii}	0.93	2.50	3.351(3)	153
O9A−H1W···O7	0.86	1.91	2.767(17)	173
O10A−H6W···O8	0.86	2.10	2.771(7)	135
N2−H2N···O9A^{iii}	0.86	2.05	2.849(18)	155
N4−H4N···O10A	0.86	1.93	2.771(6)	166
C21−H21A···O9B	0.96	2.10	2.935(6)	144

[a] Symmetry code: (i) $1-x, y, 1/2-z$; (ii) $1/2-x, -1/2+y, 1/2-z$; (iii) $1-x, 1-y, -z$; (iv) $1/2+x, -1/2+y, z$.

steric factors have been balanced since the replacement of a H atom by a $-CH_3$ group in the Schiff base ligand (differing in a $-CH_2-$ group) implies the replacement of a CH_3OH molecule by a H_2O molecule (also differing in a $-CH_2-$ group). As a consequence of these two identical changes, the two compounds present the same formula with different connectivities of the ligands and constitute a pair of structural isomers. In **3**, a hydroxyl group has been incorporated in the aromatic ring of the salicylaldehyde. This modification produces interesting electronic effects (besides the logical steric ones) giving rise to the formation of extra H-bonds (as compared with **1** and **2**). Thus, as can be observed in Scheme 1, the resulting L^3H ligand presents two −OH groups in *ortho* and *meta* to the imine functionality in the aromatic ring that act as strong H-bond donors giving rise to several H-bonds containing the O1, O2, and O5 atoms as H-bond donors and the deprotonated O4 atoms as H-bond acceptor (Table 5). On the other hand, the additional free (*meta*) −OH group withdraws electron density from the aromatic ring and, therefore, from the coordinating (*ortho*) −OH group, reducing its electronic density. This reduced electronic density in the latter −OH group may be the reason for the absence of a phenoxo bridge by the *ortho* −OH group in **3**, in contrast to **1** and **2**, leading to the formation of a monomer in **3** instead of a centrosymmetric dimer, as in **1** and **2**.

All complexes present interesting H-bonding topologies increasing from 1D to 2D and to 3D in **1**, **2**, and **3**, respectively. The differences in the H-bonding network observed between the isomeric complexes **1** and **2** may be attributed to the presence of different coordinating molecules in one of the axial positions (a CH_3OH molecule in **1** and a H_2O molecule in **2**). Thus, in **1** the methanolic proton (H1) forms an intramolecular H-bond but no intermolecular ones. In fact, the only intermolecular H-bond in **1** occurs between the amide proton (H23) of one unit with the free trifluoroacetato oxygen (O23) of an adjacent unit along the *c* axis described by the basic unitary ring graph model $R_2^2(14)$ which gives rise to a 1D chain supramolecular architecture. In case of **2** the coordinated water molecule has two protons with favorable orientations to participate in H-bonding. One of them (H15) forms an intramolecular O−H···O interaction with the trifluoroacetate moiety. The other proton (H4) forms a H-bond with the coordinated keto oxygen (O12) of a neighboring molecule, giving rise to a $R_2^2(8)$ H-bonding ring pattern that propagates along the *a* axis in addition to a $R_2^2(14)$ pattern that propagates along the *c* axis similar to **1**. This additional H-bonding ability of the water molecule in **2** generates in this compound a 2D H-bonded network in contrast to **1** where the H-bond network is limited to 1D.

In contrast to **1** and **2**, **3** has no symmetry element within the molecule and, therefore, no symmetrical intramolecular hydrogen bond is present. The presence of two lattice water molecules and one terminal hydroxyl group attached to the Schiff base makes the trifluoroacetato oxygen (O8) a trifurcated H-bond acceptor from three different directions while in **1** and **2** the trifluoroacetate oxygen (O23) is H-bonded only with the free amide proton along the *c* axis. Moreover an O−H···O $R_2^2(8)$ ring graph type is formed in **3** by purely interligand interactions between two adjacent basal-apical ligand moieties of two neighboring units because of the simultaneous coordination of one neutral and one monoanionic ligand fragments to the metal center. In **2** also an O−H···O $R_2^2(8)$ ring graph type set is present, but it involves protons from coordinated water molecules as in this compound all the coordinated ligands are deprotonated. In summary, the tiny variations introduced in the ligands (L^1H, L^2H, and L^3H) have generated important structural modifications in complexes **1**−**3**, especially in their supramolecular H-bonding architectures, passing from a 1D chain in **1** (Figure 3), to a 2D sheet in **2** (Figure 4), and to a 3D network in **3** (Figure 8).

Magnetic Properties. The thermal variation of the molar magnetic susceptibility per Ni(II) dimer times the temperature ($\chi_m T$) shows at room temperature a value of about 2.45 cm^3 K mol^{-1} for **1** and about 2.35 cm^3 K mol^{-1} for **2** (Figure 9). These values are close to the expected ones for two isolated Ni(II) $S = 1$ ions with $g = 2.21$ and 2.17, respectively. When cooling down the sample, the $\chi_m T$ product smoothly decreases from room temperature down to about 150 K. Below this temperature $\chi_m T$ shows a more pronounced decrease to reach a value of about 0.1 and 0.06 emu K mol^{-1} at about 2 K for **1** and **2**, respectively

dx.doi.org/10.1021/ic200846j |*Inorg. Chem.* 2011, 50, 8326–8339

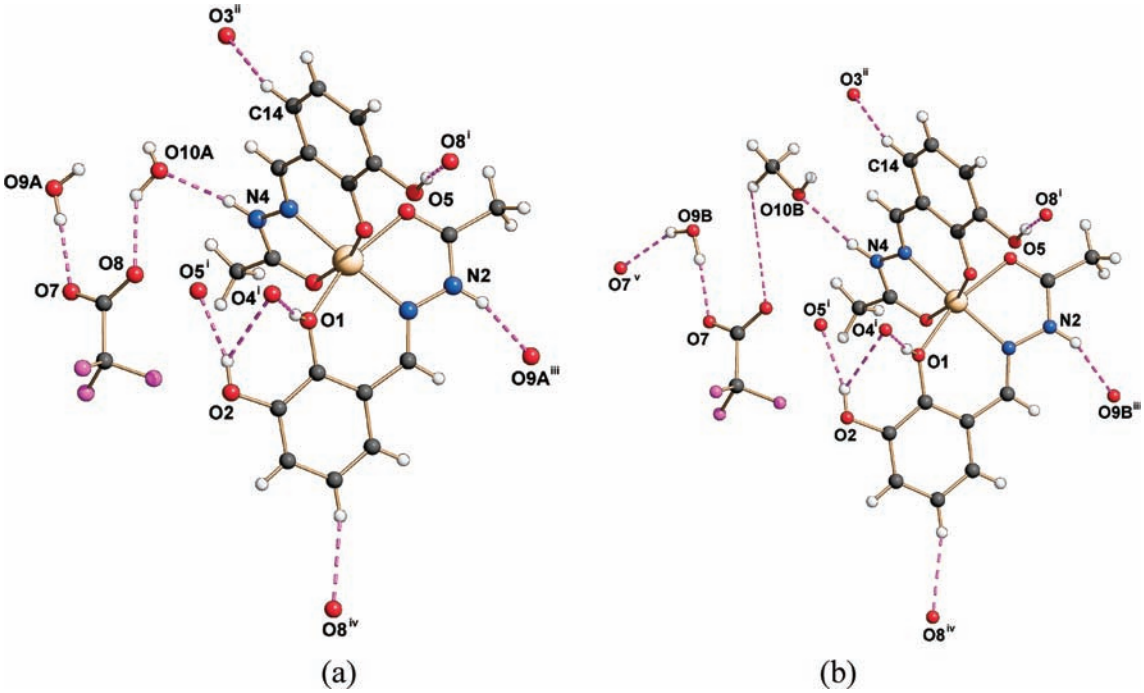

Figure 7. H-bonding network in **3** showing the two different possibilities for the solvent molecules: (a) O9A and O10A atoms and (b) O9B and O10B atoms. Only the major components of disorder are shown. Symmetry codes: (i) 1−*x*, *y*, 0.5−*z*; (ii) 1−*x*, 1−*y*, −*z*; (iii) 0.5+*x*. −0.5+*y*, *z*; (iv) 0.5−*x*, −0.5+*y*, 0.5−*z* and (v) −*x*, 1−*y*, −*z*.

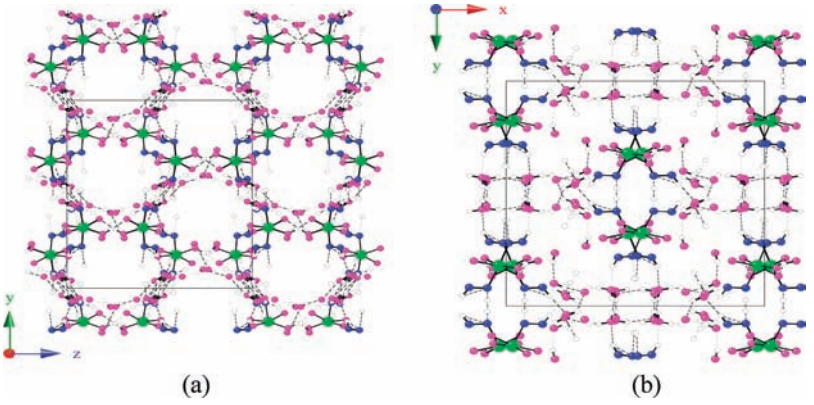

Figure 8. Crystal packing of **3** showing the 3D hydrogen bonding network in the *yz* plane (a) and *xy* plane (b). Only the atoms involved in H-bonds and the Ni atoms are shown for clarity.

(Figure 9). This behavior indicates that both **1** and **2** present moderate antiferromagnetic coupling, responsible for the progressive decrease observed below about 150 K. As expected, this moderate coupling is confirmed by the thermal variation of χ_m that shows a rounded maximum at about 25 K followed by a minimum at about 6 K and a divergence below about 6 K for **1** (inset in Figure 9a). In **2** the thermal variation of χ_m also shows a rounded maximum at about 23 K followed by a minimum at about 7.4 K and a divergence below this temperature (inset in Figure 9b). These divergences at low temperatures can be attributed to the presence of a small amount of paramagnetic monomeric Ni(II) impurity.

Since the crystal structures of both **1** and **2** consist of Ni(II) dimers connected through a double phenoxo bridge, we have fit the magnetic properties of both compounds with a simple $S = 1$ dimer model (the Hamiltonian is written as $H = -JS_iS_{i+1}$) plus a monomeric $S = 1$ paramagnetic contribution.[36]

$$\chi_m = (1-c)\frac{Ng^2\beta^2}{kT}\frac{2e^x + 10e^{3x}}{1 + 3e^x + 5e^{3x}} + (c)\frac{2Ng^2\beta^2}{3kT} \quad with \quad x = J/kT$$

This model reproduces very satisfactorily the magnetic data of both complexes in the whole temperature range with $g = 2.250(2)$, $J = -19.2(1)$ cm^{-1} and a monomeric impurity of $c = 4.6(1)$ % for **1** (solid line in Figure 9a) and $g = 2.136(1)$, $J = -19.5(1)$ cm^{-1} and a monomeric impurity of $c = 2.8(1)$ % for **2** (solid line in Figure 9b). Note that the antiferromagnetic

dx.doi.org/10.1021/ic200846j |*Inorg. Chem.* 2011, 50, 8326–8339

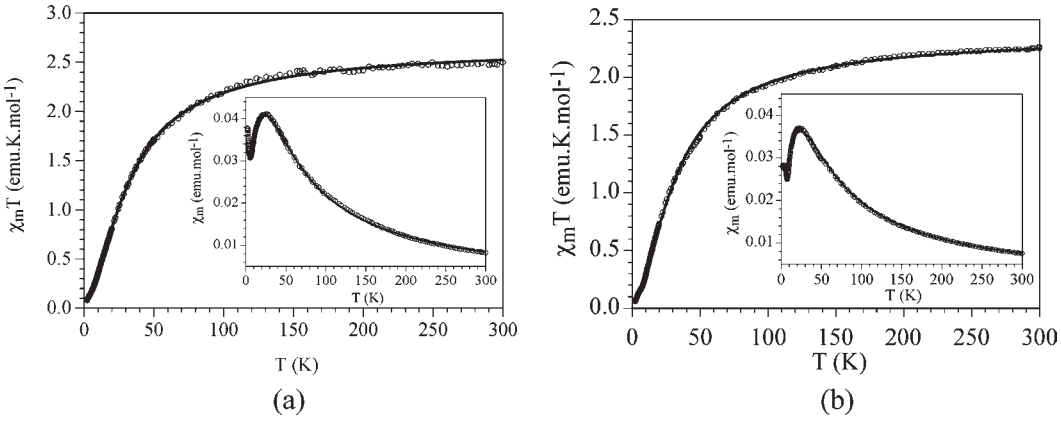

Figure 9. Thermal variation of the $\chi_m T$ product per Ni(II) dimer for **1** (a) and for **2** (b). Inset shows the thermal variation of χ_m. Solid line is the best fit to the $S = 1$ dimer model with a paramagnetic impurity (see text).

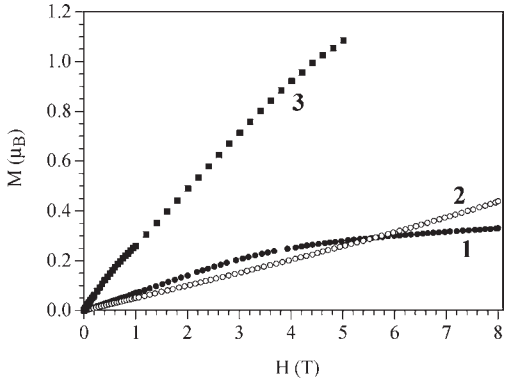

Figure 10. Isothermal magnetization at 2 K for compounds **1**−**3** per Ni(II) dimer.

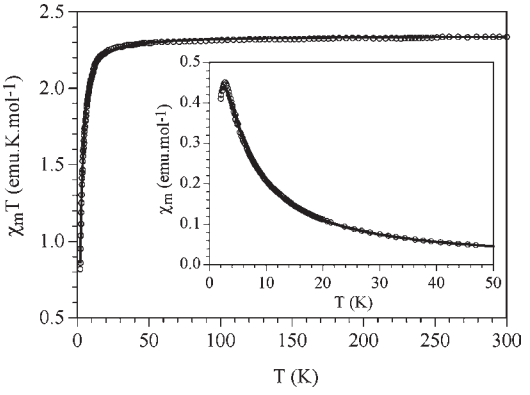

Figure 11. Thermal variation of the $\chi_m T$ product per two Ni(II) ions for **3**. Inset shows the thermal variation of χ_m. Solid line is the best fit to the $S = 1$ dimer model with a ZFS (see text).

J value may also include a zero field splitting (ZFS) of the $S = 1$, Ni(II) ions.

A further confirmation of the overall antiferromagnetic coupling is provided by the isothermal magnetization at 2 K that shows almost linear field dependence up to fields of about 3.5 T and shows an almost saturation even at 8 T (Figure 10). At 8 T the magnetization value is about 0.33 μ_B for **1** and about 0.40 μ_B for **2**, well below the expected value for two noninteracting $S = 1$ Ni(II) ions (ca. 4.5 μ_B for $g = 2.25$), confirming the presence of antiferromagnetic interactions in these compounds. The more linear behavior observed in **2** indicates that in this compound the amount of monomeric Ni(II) impurity is lower than in **1**, in agreement with the behavior of the $\chi_m T$ product at low temperatures.

The thermal variation of the $\chi_m T$ product per two Ni(II) ions for **3** shows at room temperature a value of about 2.33 cm^3 K mol^{-1}, which is the expected value for two independent Ni(II) ions with a g factor of about 2.16. When the sample is cooled, the $\chi_m T$ value remains constant down to about 20 K and then shows a progressive decrease to reach a value of about 0.8 cm^3 K mol^{-1} at 2 K (Figure 11). This behavior suggests that **3** presents a weak, although not negligible, antiferromagnetic coupling, as is confirmed by the thermal variation of the molar magnetic susceptibility (χ_m) that shows a maximum at about 3 K (inset in Figure 11). Although a first look at the structure of **3** shows the presence of isolated Ni(II) complexes with two Shiff-base ligands connected with the *mer* configuration, a close look at the structure of **3** shows that these Ni(II) monomers aggregate to form H-bonded dimers where the aromatic rings stack parallel with a short interplanar distance and a $\pi-\pi$ stacking interaction is operated between the aromatic rings of one complex with those of the other complex (Figure 6). According to this dimerization, we have fit the magnetic properties of **3** to the same simple $S = 1$ dimer model that we have used for **1** and **2**. Unfortunately, this model gives a very low J value (as expected) which is not able to reproduce the more pronounced decrease observed in $\chi_m T$ at very low temperatures. This fact suggests that, given the very low J value present in the compound, it is also necessary to include a ZFS in the $S = 1$ monomers.[37] This model satisfactorily reproduces the magnetic properties of **3** in the whole temperature range with the following set of parameters: $g = 2.06(3)$, $J = -0.60(2)$ cm^{-1}, and $|D| = 3.4(2)$ cm^{-1} (solid line in Figure 11). Note that both parameters, D and J, are correlated, and, therefore, these values might be over or underestimated. Nevertheless, the D value is within the normal range observed in similar octahedral Ni(II) complexes.[37b]

A further confirmation of the weak antiferromagnetic coupling in **3** is provided by the isothermal magnetization at 2 K that shows a linear dependence with the magnetic field with a value of 1.1 μ_B at 5 T and no saturation (Figure 10). This value is well below the expected value of about 2.1 μ_B for an isolated Ni(II)

dx.doi.org/10.1021/ic200846j |*Inorg. Chem.* 2011, 50, 8326–8339

complex. Note that the magnetization in **3** is above those of **1** and **2** [in all cases the magnetization represented in Figure 10 corresponds to a Ni(II) dimer]. This result agrees with the lower antiferromagnetic coupling found in **3** when compared with **1** and **2**.

As already described in the structural section, **1** and **2** are Ni(II) dimers with a double phenoxo bridge. Magneto-structural correlations for such Ni(II) complexes with double phenoxo bridges indicate that the most important parameter controlling the exchange coupling is the Ni−O−Ni bond angle. Thus, when this angle is close to 90° the coupling is ferromagnetic, and it decreases as the angle becomes larger with a crossing point to antiferromagnetic coupling near 97−98°.[38] In **1** and **2** the Ni−O−Ni bond angles are both very similar [98.74(12)° and 99.06(15)°, respectively] and slightly above the crossing point and, therefore, the magnetic coupling is expected to be weak and antiferromagnetic for both compounds, in agreement with the experimental data.

A second structural parameter that has also been claimed to play an important role in determining the magnetic coupling in these doubly phenoxo bridged Ni(II) complexes is the torsion Ni−O−O−Ni angle. For angles above about 170° an antiferromagnetic coupling is anticipated.[38c] In case of **1** and **2** the Ni−O−O−Ni torsion angles are 180° (since both dimers are centrosymmetric). From previous magneto-structural correlations,[38c] this torsion angle is expected to give rise to an exchange coupling constant close to $-20\ cm^{-1}$, in excellent agreement with the experimental results in both complexes.

Finally the magnetic coupling must include the zero field splitting (ZFS) expected for Ni(II) complexes. In fact, the thermal variation of $\chi_m T$ shows that the theoretical models are above the experimental points at very low temperatures. Unfortunately, all the attempts to fit the magnetic data of both compounds with a $S = 1$ dimer model including a ZFS led to unrealistic J and D parameters since they are strongly correlated.[37] Furthermore, the presence of a paramagnetic impurity also precludes the determination of realistic D parameters in both compounds given its strong influence at low temperatures.

In **3** the situation is different since now the very weak magnetic coupling is due to the presence of hydrogen bonding and $\pi-\pi$ stacking interaction that leads to a short interplanar distance between the aromatic rings of the Shiff base ligands of two symmetry-related monomers (Figure 6). Such weak interactions, already observed in other similar Ni(II) monomers with Shiff base ligands,[39] are expected to give rise to very weak antiferromagnetic coupling since density functional theory (DFT) calculations in a similar Ni(II) monomer show that most of the spin density is located on the Ni(II) ions with a weak delocalization on the aromatic rings.[40]

Catalytic Epoxidation of Alkenes. The effect of different oxidants on the catalytic activity of **1**, **2**, and **3** in the oxidation of styrene, *cis*-stylbene, cyclohexene, and *trans*-4-octene was evaluated. When PhIO in acetonitrile, H_2O_2 in 1:1 acetone/H_2O or O_2/aldehyde in Cl_2CH_2 were used as the oxygen source, no oxidation products were detected in the reaction mixtures, even when increasing the temperature, reaction time, oxidant, or catalyst concentrations. However, **1**, **2**, and **3** showed activity to catalyze the oxidation of *cis*-stylbene, cyclohexene, *trans*-4-octene, and styrene in a Cl_3CH/H_2O biphasic medium in the presence of benzyltributylammonium chloride as phase transfer catalyst (PTC) using NaOCl as oxidant. It was observed that at 20 °C, the four investigated alkenes were selectively oxidized to the epoxide. Conditions used for epoxidation by this catalytic system are summarized in Table 6. Maximal conversion was reached after 6 h; increase of the reaction time did not result in higher yields of epoxide, probably because of catalyst inactivation. In the biphasic reaction system, the three complexes are mainly present in the interphase and in the aqueous layer. This is supported by the colored aqueous layer and interphase in comparison with the colorless organic layer. During the reaction, the color of the catalyst changed from green to deep blue, and after 6 h it turned to beige. The presence of the complex in the aqueous layer was confirmed by UV−vis spectra of samples of the upper layer taken immediately after mixing and 30 min after the beginning of the reaction (as shown for **1** in Figure 12). The change in the spectral pattern means that the starting complex transforms into another species during the reaction. Ligand dissociation can be disregarded since the observed bands differ from those of the free ligand. Moreover, the shift of the ligand-to-metal charge transfer (LMCT) band to shorter wavelengths suggests structural and electronic changes from the starting high-spin complex to a higher valence or low-spin one. In the case of the dinuclear complexes **1** and **2**, the IR data of the solid recovered at the end of the reaction (Figure 13) show that ligated trifluoroacetate groups were displaced from the axial sites

Table 6. Oxidation of Alkenes with Hypochlorite Catalyzed by 1, 2, and 3[a,b]

alkene	catalyst	conversion (%)	t.o.n.[c]
cis-stylbene	**1**	13	5
	2	25	10
	3	28	11
styrene	**1**	19	8
	2	29	12
	3	33	13
cyclohexene	**1**	15	6
	2	26	10
	3	30	12
trans-4-octene	**1**	18	7
	2	30	12
	3	35	14

[a] Reaction conditions: alkene (0.4 mmol); catalyst (10 μmol); OCl^- (1.4 mmol); Cl_3CH (2 mL)/H_2O (2 mL); $T = 20°C$; $t = 6$ h, pH = 12. [b] Oxidation product: epoxide. [c] t.o.n.: amount of epoxide/amount of catalyst.

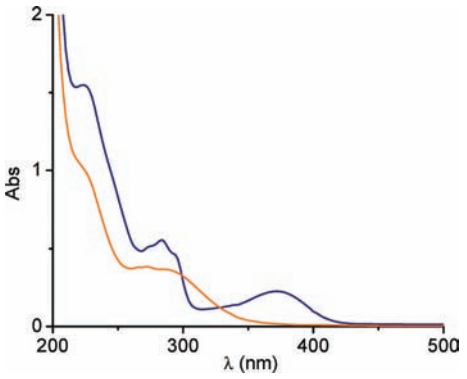

Figure 12. UV−vis spectra of **1** in water (blue) and the aqueous layer (red) after 30 min of reaction.

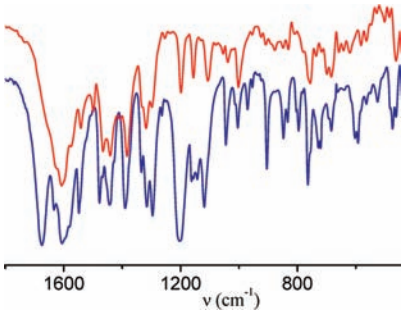

Figure 13. IR spectra of **1** (blue) and solid (red) recovered at the end of the reaction.

Table 7. Influence of the pH on the Oxidation of Styrene with OCl^- Catalyzed by 1, 2, and 3[a]

catalyst	conversion (%)	t.o.n.[b]	pH
2	29[c]	12	12
2	32[c]	13	11
2	45[c]	18	10
2	98[c]	39	9
2	82[d]	328	9
	80	320	9[e]
1	80[d]	320	9
	79	316	9[e]
3	99[d]	396	9
	95	380	9[e]

[a] Oxidation product: epoxide. Reaction conditions: styrene (0.4 mmol); OCl^- (1.4 mmol); Cl_3CH (2 mL)/H_2O (2 mL of buffered solution); T = 20°C. [b] t.o.n.: amount of epoxide/amount of catalyst. [c] t = 6 h, catalyst (10 μmol). [d] t = 2 h, catalyst (1 μmol). [e] 2nd addition of alkene.

during the reaction and that the ligand is still bound to the metal in the final form of the complex.

A study of the influence of pH on the amount of epoxide generated in the epoxidation of styrene catalyzed by **2** was undertaken to optimize the conversion to the epoxide. The results are summarized in Table 7. As it can be seen, turnover numbers increase as the pH decreases, up to 98% conversion to epoxide after 6 h at pH 9. If the amount of catalyst was decreased to 1 μmol, the maximum turnover reached 328 providing 82% yield of epoxide after 2 h. The blank reactions at this pH (i) without the Ni complex as well as (ii) without the ligand, that is, in the presence of $Ni(NO_3)_2$, resulted in the formation of 20% and 24% epoxide, respectively, after 6 h. The efficiency of the three catalysts to oxidize styrene was compared at pH 9. At this pH, **3** showed to be more efficient than the dinuclear catalysts, yielding 99% conversion to epoxide with turnover of 396 after 2 h of reaction. At this pH, the three catalysts showed to be active after complete conversion of the alkene, since a new addition of alkene resulted in conversion to epoxide with retention of efficiency (similar t.o.n. and conversion for the first and second addition of styrene). As shown in Tables 6 and 7, at pH 12, complexes **2** and **3** are better than **1** to oxidize alkenes with OCl^-, while at pH 9, **3** is the best among the three catalysts.

From the basic spectroscopic studies and pH control experiments, we can anticipate that, on lowering the pH, more HOCl is formed in the medium which helps in efficient catalysis with Ni(II) complexes. Formation of HOCl in a pH 9 aqueous

Scheme 2. Possible Mechanism for the Epoxidation of Alkenes by NaOCl with the Ni(II) Complexes

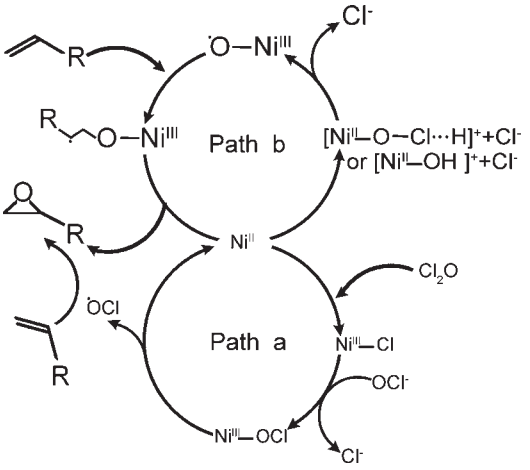

solution and benzyltributylammonium chloride assisted phase transfer of HClO to $CHCl_3$ medium could operate to provide sufficient concentration of HClO in the organic phase for effective epoxidation of alkenes. In the organic phase, two possible mechanisms are predictable based on some previous works reported by Burrows et al. and also by Freire et al.[41] On lowering the pH, sufficient amount of dichlorine monoxide is formed according to the reaction:

$$2HClO \leftrightarrow Cl_2O + H_2O \quad (1)$$

Reaction of Cl_2O with **1** and **2** would likely generate a Ni^{III}—Cl entity by the axial displacement of the trifluoroacetate moiety, and in case of **3**, such complex entity could be formed through ligand shift facilitated by ligand protonation at lower pH. The Ni^{III}—Cl complex may exchange Cl^- for ClO^-, and homolytic cleavage of Ni^{III}—OCl bond would generate ClO·, an effective epoxidising agent [path a, Scheme 2]. Another alternative possibility is the formation of higher valent Ni^{III}-oxo radical that can provide a competitive pathway toward formation of epoxide [path b, Scheme 2]. The formation of Ni^{III}—OCl or Ni^{III}—O· intermediates is dependent upon the nature of the ligand field and lability of the terminal oxidants. Indirect evidence in favor of the formation of the higher valent species lies in the blue shift of the LMCT band of the starting complex during the catalytic reaction (Figure 12).

Considering that the axial approach of the oxidant to the metal center is needed for the formation of a high valent intermediate, the steric factors around Ni must be of major importance. This explains the fact that the dinuclear complexes, with reduced steric hindrance around the metal center, are appropriate to catalyze epoxidation by ClO^-. In the case of the mononuclear Ni(II) complex, initial ClO^- attack is enforced to occur through ligand shift, which may be facilitated by protons. Therefore, at low pH, **3** is more reactive than **1** and **2**.

The activity shown by the present Ni(II)-hydrazone catalysts for alkenes oxidation with ClO^- at pH 9 is higher than that found for reported mono- and dinuclear nickel(II) Schiff-base,[19j,20,41] mononuclear Ni(II)-multiazamacrocyclic,[19d] and porphyrinic[19j] complexes. Besides, the 100% selectivity of the present Ni(II) complexes for catalytic epoxidation with ClO^-

dx.doi.org/10.1021/ic200846j |*Inorg. Chem.* 2011, 50, 8326–8339

strongly differentiates these complexes from the more conventional systems based on salen and other Schiff base ligands,[19j,41,42] for which selectivity ranges from 15 to 45% depending on the alkene. Therefore, the present results show that Ni(II)-hydrazone complexes satisfy ligand requirements for acceptable activity and high selectivity in the epoxidation of alkenes with ClO^-.

CONCLUSION

We have explored the important structural modifications observed in three octahedral Ni(II) complexes originated by small variations of a Shiff base ligand with a potentially tridentate ONO donor hydrazone moiety. These Shiff base ligands have been modified only in the carbonyl function while keeping the amine part intact. Thus, in ligand L^1H the carbonyl group carries a H atom that reduces the steric hindrance allowing the coordination of a CH_3OH molecule to complete the coordination sphere of the Ni(II) ion in **1**. In contrast, the inclusion of a $-CH_3$ in the carbonyl group (in L^2H) has led to a more sterically hindered **2**, where a water molecule has replaced the CH_3OH ligand, (leading to a couple of unusual complex isomers **1** and **2**). Interestingly, this change implies a higher ability of **2** to form H-bonds as shown by the 2D H-bonded network present in **2** (with $R_2^2(8)$ and $R_2^2(14)$ motifs) compared to the 1D H-bonded network in **1** (with a $R_2^2(14)$ motif). A second modification has led to the synthesis of L^3H where we have included electronic effects in the ligand with an electron withdrawing −OH group in *meta* position in addition to the *ortho* −OH group with respect to the azomethine functionality in the aromatic ring of the Schiff base ligand. This second −OH group seems to be at the origin of the absence of a double phenoxo bridge in **3** (which was present in **1** and **2**) precluding the formation of a Ni(II) dimer. The unusual presence of a protonated L^3H ligand in **3** increases the number of H-bonds and leads to the formation of a 3D H-bonded network in this complex (with a $R_2^2(8)$ motif). Although **3** is a Ni(II) monomeric complex with two Schiff base ligands, the *mer* disposition of these two ligands leads to a H-bonded dimer with short interplanar contacts between the aromatic rings of two adjacent complexes, leading to the association of the molecules with $\pi-\pi$ overlap. The magnetic properties of the three complexes (moderate antiferromagnetic coupling in **1** and **2** and very weak one in **3**) are easily explained from the structural parameters of the double phenoxo bridges and the hydrogen bonding as well as the $\pi-\pi$ interactions. All the Ni(II)-hydrazone complexes are active catalysts in the epoxidations of *cis*-stylbene, styrene, cyclohexene, and *trans*-4-octene by NaOCl under phase transfer conditions. Conversions up to 99% and TON up to 396 are obtained at reduced pH implying the intermediacy of a high valent nickel−oxygen species, either $Ni^{III}-OCl$ or $Ni^{III}-O^{\cdot}$, whose formation is facilitated by the displacement of labile terminal CF_3COO^- moiety in **1** and **2** and by the proton assisted ligand shift in **3**.

ASSOCIATED CONTENT

Supporting Information. X-ray crystallographic files including the structural data for **1**, **2**, and **3** in CIF format. Detailed discussion about the FT-IR, UV−vis, and ESI mass spectroscopic studies of the ligands and the complexes. This material is available free of charge via the Internet at http://pubs.acs.org.

AUTHOR INFORMATION

Corresponding Author

*Phone: +91 033 2414 6666, x 2779. Fax: +91 033 2414 6414. E-mail: smitra_2002@yahoo.com.

ACKNOWLEDGMENT

D.S. thanks the University Grants Commission, New Delhi, Government of India, for financial support. D.S. is also very thankful to Dr. Sambuddha Banerjee, Department of Chemistry, Duke University, for thoughtful discussions on this project. C.J.G. acknowledges the European Union for financial support (MAGMANet network of excellence), the Spanish Ministerio de Educación y Ciencia (Projects MAT2007-61584 and CSD 2007-00010 Consolider-Ingenio in Molecular Nanoscience), and the GeneralitatValenciana (Project PROMETEO/2009/095).

REFERENCES

(1) (a) Lehn, J. M., Ed.; *Supramolecular Chemistry, Concepts and Perspectives*; VCH: Weinheim, Germany, 1995. (b) Philip, D.; Stoddart, J. F. *Angew. Chem., Int. Ed. Engl.* **1996**, *35*, 1155–1196. (c) Balzani, V.; Gedi, A.; Raymo, F. M.; Stoddart, J. F. *Angew. Chem., Int. Ed.* **2000**, *39*, 3348–3391.

(2) (a) *Inorganic Crystal Engineering, Dalton Discussion No. 3, J. Chem. Soc., Dalton Trans.*, **2000**, 3705−3998. (b) Zaworotko, M. J. *Angew. Chem., Int. Ed.* **2000**, *39*, 3052–3054.(c) Haiduc, I.; Edelmann, F. T. *Supramolecular Organometallic Chemistry*; Wiley-VCH: Weinheim, Germany, 1999.

(3) Steiner, T. *Angew. Chem., Int. Ed.* **2002**, *41*, 48–76.

(4) Rao, C. N. R. *Curr. Sci.* **2001**, *81*, 1030–1037.

(5) (a) Ma, J. C.; Dougherty, D. A. *Chem. Rev.* **1997**, *97*, 1303–1324. (b) Gallivan, J. P.; Dougherty, D. A. *Proc. Natl. Acad. Sci. U.S.A.* **1999**, *96*, 9459–9464. (c) Dougherty, D. A. *Science* **1996**, *271*, 163–168. (d) Gallivan, J. P.; Dougherty, D. A. *J. Am. Chem. Soc.* **2000**, *122*, 870–874.

(6) Jeffrey, G. A. *An introduction to hydrogen bonding*; Oxford University Press; Oxford, England, 1997.

(7) (a) Desiraju, G. R. *Crystal Engineering. The Design of Organic Solids*; Elsevier: Amsterdam, The Netherlands, 1989. (b) Lawrence, D. S.; Jiang, T.; Levitt, M. *Chem. Rev.* **1995**, *95*, 2229–2260.

(8) El-ghayoury, A.; Peeters, E.; Schenning, A. P. H. J.; Meijer, E. W. *Chem. Commun.* **2000**, 1969–1970.

(9) (a) Bell, T. W.; Hou, Z. *Angew. Chem., Int. Ed.* **1997**, *36*, 1536–1538. (b) Chang, S. K.; Van Engen, D.; Fan, E.; Hamilton, A. D. *J. Am. Chem. Soc.* **1991**, *113*, 7640–7645.

(10) (a) Rebek, J., Jr. *Chem. Soc. Rev.* **1996**, *25*, 255–264. (b) Conn, M. M.; Rebek, J., Jr. *Chem. Rev.* **1997**, *97*, 1647–1668. (c) Hof, F.; Craig, S. L.; Nuckolls, C.; Rebek, J., Jr. *Angew. Chem., Int. Ed.* **2002**, *41*, 1488–1508.

(11) Bong, D. T.; Clark, T. D.; Granja, J. R.; Ghadiri, M. R. *Angew. Chem., Int. Ed.* **2001**, *40*, 988–1011.

(12) (a) Etter, M. C. *Acc. Chem. Res.* **1990**, *23*, 120–126. (b) Etter, M. C.; MacDonald, J. M.; Bernstein, J. *Acta Crystallogr., Sect. B* **1990**, *46*, 256–262. (c) Bernstein, J.; Shimoni, L.; Davis, R. E.; Chang, N.-L. *Angew. Chem., Int. Ed. Engl.* **1995**, *34*, 1555–1573.

(13) (a) Chitrapriya, N.; Mahalingam, V.; Zeller, M.; Natarajan, K. *Inorg. Chim. Acta* **2010**, *363*, 3685–3693. (b) Stadler, A.-M.; Puntoriero, F.; Nastasi, F.; Campagna, S.; Lehn, J.-M. *Chem.—Eur. J.* **2010**, *16*, 5645–5660. (c) Angelusiu, M. V.; Barbuceanu, S.-F.; Draghici, C.; Almajan, G. L. *Eur. J. Med. Chem.* **2010**, *45*, 2055–2062. (d) Pyta, K.; Przybylski, P.; Huczyński, A.; Hoser, A.; Woźniak, K.; Schilf, W.; Kamieński, B.; Grech, E.; Brzezinski, B. *J. Mol. Struct.* **2010**, *970*, 147–154. (e) Pedrido, R.; Romero, M. J.; Bermejo, M. R.; González-Noya, A. M.; Maneiro, M.; Jesús Rodríguez, M.; Zaragoza, G. *Dalton Trans.* **2006**, 5304–5314 and references cited therein. (f) Sangeetha, N. R.; Pal, S. *Polyhedron* **2000**, *19*, 1593–1600 and references cited therein. (g) Palamarciuc, O. V.; Bourosh, P. N.; Revenco, M. D.; Lipkowski, J.; Simonov, Y. A.; Clérac, R. *Inorg. Chim.*

Acta **2010**, *363*, 2561–2566. (h) Guskos, N.; Likodimos, V.; Glenis, S.; Typek, J.; Wabia, M.; Paschalidis, D. G.; Tossidis, I.; Lin, C. L. *J. Magn. Magn. Mater.* **2004**, *272*−*276*, 1067–1069. (i) Viñuelas-Zahínos, E.; Luna-Giles, F.; Torres-García, P.; Bernalte-García, A. *Polyhedron* **2009**, *28*, 1362–1368. (j) Filipović, N.; Borrmann, H.; Todorović, T.; Borna, M.; Spasojević, V.; Sladić, D.; Novaković, I.; Andjelković, K. *Inorg. Chim. Acta* **2009**, *362*, 1996–2000.

(14) (a) Banerjee, S.; Mondal, S.; Sen, S.; Das, S.; Hughes, D. L.; Rizzoli, C.; Desplanches, C.; Mandal, C.; Mitra, S. *Dalton Trans.* **2009**, 6849–6860. (b) Banerjee, S.; Sen, S.; Chakraborty, J.; Butcher, R. J.; Gómez-García, C. J.; Puchta, R.; Mitra, S. *Aust. J. Chem.* **2009**, *62*, 1614–1621. (c) Chakraborty, J.; Thakurta, S.; Pilet, G.; Luneau, D.; Mitra, S. *Polyhedron* **2009**, *28*, 819–825. (d) Ray, A.; Rizzoli, C.; Pilet, G.; Desplanches, C.; Garribba, E.; Rentschler, E.; Mitra, S. *Eur. J. Inorg. Chem.* **2009**, *20*, 2915–2928. (e) Ray, A.; Banerjee, S.; Butcher, R. J.; Desplanches, C.; Mitra, S. *Polyhedron* **2008**, *27*, 2409–2415. (f) Banerjee, S.; Ray, A.; Sen, S.; Mitra, S.; Hughes, D. L.; Butcher, R. J.; Batten, S. R. *Inorg. Chim. Acta* **2008**, *361*, 2692–2700 and references cited therein. (g) Banerjee, S.; Sen, S.; Basak, S.; Mitra, S.; Hughes, D. L.; Desplanches, C. *Inorg. Chim. Acta* **2008**, *361*, 2707–2714. (h) Samanta, B.; Chakraborty, J.; Shit, S.; Batten, S. R.; Jensen, P.; Masuda, J. D.; Mitra, S. *Inorg. Chim. Acta* **2007**, *360*, 2471–2484. (i) Sen, S.; Choudhury, C. R.; Talukder, P.; Mitra, S.; Westerhausen, M.; Kneifel, A. N.; Desplanches, C.; Daro, N.; Sutter, J.-P. *Polyhedron* **2006**, *25*, 1271–1278. (j) Sen, S.; Mitra, S.; Hughes, D. L.; Rosair, G.; Desplanches, C. *Polyhedron* **2007**, *26*, 1740–1744.

(15) (a) Kashar, T. I. *Thermochim. Acta* **2010**, *507*−*508*, 66–70. (b) AbouEl-Enein, S.; El-Saied, F. A.; Emam, S. M.; Ell-Salamony, M. A. *Spectrochim. Acta, Part A* **2008**, *71*, 421–429. (c) Chan, S. C.; Koh, L. L.; Leung, P.-H.; Ranford, J. D.; Sim, K. Y. *Inorg. Chim. Acta* **1995**, *236*, 101–108. (d) Ainscough, E. W.; Brodie, A. M.; Dobbs, A. J.; Ranford, J. D.; Waters, J. M. *Inorg. Chim. Acta* **1998**, *267*, 27–38. (e) Pal, S.; Pal, S. *Eur. J. Inorg. Chem.* **2003**, 4244–4252.

(16) (a) Banerjee, S.; Nandy, M.; Sen, S.; Mandal, S.; Rosair, G. M.; Slawin, A. M. Z.; Gómez-García, C. J.; Clemente-Juan, J. M.; Zangrando, E.; Guidolin, N.; Mitra, S. *Dalton Trans.* **2011**, *40*, 1652–1661. (b) Mukherjee, P.; Drew, M. G. B.; Gómez-García, C. J.; Ghosh, A. *Inorg. Chem.* **2009**, *48*, 5848–5860. (c) Mukherjee, P.; Drew, M. G. B.; Tangoulis, V.; Estrader, M.; Diaz, C.; Ghosh, A. *Inorg. Chem. Commun.* **2009**, *12*, 929–932. (d) Bu, X.-H.; Du, M.; Zhang, L.; Liao, D.-Z.; Tang, J.-K.; Zhang, R.-H. *Dalton Trans.* **2001**, 593–598. (e) Banerjee, A.; Singh, R.; Chopra, D.; Colacio, E.; Rajak, K. K. *Dalton Trans.* **2008**, 6539–6545.

(17) Canali, L.; Sherrington, D. C. *Chem. Soc. Rev.* **1999**, *28*, 85–93.

(18) (a) Jacobsen, E. N.; Pfaltz, A.; Yamamoto, H. *Comprehensive Asymmetric Catalysis*; Springer: Berlin, Germany, 1999, Vol. III. (b) Nishikori, H.; Ohta, C.; Katsuki, T. *Synlett* **2000**, 1557–1560. (c) Sabater, M. J.; Corma, A.; Domenech, A.; Fornés, V.; García, H. *Chem. Commun.* **1997**, 1285–1286.

(19) (a) Mirkhani, V.; Moghadam, M.; Tangestaninejad, S.; Baltork, I. M.; Shams, E.; Rasouli, N. *Appl. Catal., A* **2008**, *334*, 106–111. (b) Xia, Q.-H.; Ge, H.-Q.; Ye, C.-P.; Liu, Z.-M.; Su, K.-X. *Chem. Rev.* **2005**, *105*, 1603–1662. (c) Kureshy, R. I.; Khan, N. H.; Abdi, S. H. R.; Patel, S. T.; Iyer, P.; Suresh, E.; Dastidar, P. *J. Mol. Catal. A: Chem.* **2000**, *160*, 217–227. (d) Lee, D.; Bang, H.; Suh, M. P. *J. Mol. Catal. A: Chem.* **2000**, *151*, 71–78. (e) Kureshy, R. I.; Khan, N. H.; Abdi, S. H. R.; Iyer, P.; Bhatt, A. K. *J. Mol. Catal. A: Chem.* **1998**, *130*, 41–50. (f) Fernández, I.; Pedro, J. R.; Rosalló, A. L.; Ruiz, R.; Ottenwaelder, X.; Journaux, Y. *Tetrahedron Lett.* **1998**, *39*, 2869–2872. (g) Nam, W.; Kim, S. H.; Kim, S. J.; Ho, R. Y. N.; Valentine, J. S. *Inorg. Chem.* **1996**, *35*, 1045–1049. (h) Nam, W.; Valentine, J. S. *J. Am. Chem. Soc.* **1993**, *115*, 1772–1778. (i) Kinneary, J. F.; Wagler, T. R.; Burrows, C. J. *Tetrahedron Lett.* **1988**, *29*, 877–880. (j) Yoon, H.; Burrows, C. J. *J. Am. Chem. Soc.* **1988**, *110*, 4087–4089. (k) Kinneary, J. F.; Albert, J. S.; Burrows, C. J. *J. Am. Chem. Soc.* **1988**, *110*, 6124–6129.

(20) Rispens, M. T.; Gelling, O. J.; Vries, A. H. M. D.; Meetsma, A.; Bolhuis, F. V.; Feringa, B. L. *Tetrahedron* **1996**, *52*, 3521–3546.

(21) *COLLECT*; Nonius BV: Delft, The Netherlands, 1997−2001.

(22) *APEX2*, Version 2.1; *Area Detector Control and Integration Software*, v. 6.45; Bruker Analytical X-Ray Instruments, Inc.: Madison, WI, 2006.

(23) *SMART and SAINT*; Bruker AXS Inc.: Madison, WI, 1998.

(24) Otwinowski, Z.; Minor, W. Methods in Enzymology. In *Macromolecular Crystallography, Part A*; Carter, C. W., Jr., Sweet, R. M., Eds.; Academic Press: New York, 1997; Vol. 276, pp 307−326.

(25) *Saint, Area-Detector Integration Software*; Siemens Industrial Automation, Inc.: Madison, WI, 1995.

(26) *SADABS, Program for absorption corrections using Siemens CCD based on the method of Blessing*; Blessing, R. H. *Acta Crystallogr.* **1995**, *A51*, 33.

(27) Altomare, A.; Burla, M. C.; Camalli, M.; Cascarano, G. L.; Giacovazzo, C.; Guagliardi, A.; Moliterni, A. G. G.; Polidori, G.; Spagna, R. *J. Appl. Crystallogr.* **1999**, *32*, 115–119.

(28) Sheldrick, G. M. *SHELX-97*; University of Göttingen: Göttingen, Germany, 1997.

(29) Watkin, D. J.; Prout, C. K.; Carruthers, J. R.; Betteridge, P. W. *CRYSTALS*, Issue 11; Chemical Crystallography Laboratory: Oxford, U. K., 1999.

(30) Liua, H.; Wanga, H.; Niua, D.; Lua, Z.; Sunb, J. *Synth. React. Inorg., Met.-Org., Nano-Met. Chem.* **2005**, *35*, 233–236.

(31) Nanda, K. K.; Das, R.; Thompson, L. K.; Venkatsubramanian, K.; Paul, P.; Nag, K. *Inorg. Chem.* **1994**, *33*, 1188–1193.

(32) Thakurta, S.; Chakraborty, J.; Rosair, G.; Butcher, R. J.; Mitra, S. *Inorg. Chim. Acta* **2009**, *362*, 2828–2836.

(33) Majumder, A.; Rosair, G. M.; Mallick, A.; Chattopadhyay, N.; Mitra, S. *Polyhedron* **2006**, *25*, 1753–1762.

(34) Samanta, B.; Chakraborty, J.; Shit, S.; Batten, S. R.; Jensen, P.; Masuda, J. D.; Mitra, S. *Inorg. Chim. Acta* **2007**, *360*, 2471–2484.

(35) Banerjee, S.; Mondal, S.; Chakraborty, W.; Sen, S.; Gachhui, R.; Butcher, R. J.; Slawin, A. M. Z.; Mandal, C.; Mitra, S. *Polyhedron* **2009**, *28*, 2785–2793.

(36) O'Connor, C. J. *Prog. Inorg. Chem.* **1982**, *29*, 203–283.

(37) (a) Ginsberg, A. P.; Martin, R. L.; Brookes, R. W.; Sherwood, R. C. *Inorg. Chem.* **1972**, *11*, 2884–2891. (b) Boca, R. *Coord. Chem. Rev.* **2004**, *248*, 757–815.

(38) (a) Halcrow, M. A.; Sun, J. S.; Huffman, J. C.; Christou, G. *Inorg. Chem.* **1995**, *34*, 4167–4177. (b) Clemente-Juan, J. M.; Coronado, E.; Galán-Mascarós, J. R.; Gómez-García, C. J. *Inorg. Chem.* **1999**, *38*, 55–63. (c) Clemente-Juan, J. M.; Chansou, B.; Donnadieu, B.; Tuchages, J. P. *Inorg. Chem.* **2000**, *39*, 5515–1519. (d) Mukherjee, P.; Drew, M. G. B.; Gómez-García, C. J.; Ghosh, A. *Inorg. Chem.* **2009**, *48*, 5848–5860.

(39) (a) Lu, T.-B.; Xiang, H.; Luck, R. L.; Maoa, Z.-W.; Chen, X.-M.; Ji, L.-N. *Inorg. Chim. Acta* **2009**, *355*, 229–241. (b) Shi, Q.; Sun, Y.; Sheng, L.; Maa, K.; Cai, X.; Liu, D. *Inorg. Chim. Acta* **2009**, *362*, 4167–4173. (c) Li, X.-Z.; He, J.-H.; Liu, B.-L.; Liao, D.-Z. *Inorg. Chem. Commun.* **2004**, *7*, 420–422. (d) Zhang, D.; Weng, L.; Jin, G.-X. *J. Organomet. Chem.* **2010**, *695*, 643–647.

(40) Xu, H.; Ni, Z. P.; Ren, X. M.; Meng, Q. J. *J. Mol. Struct.* **2005**, *752*, 153–157.

(41) (a) Yoon, H.; Wagler, T. R.; O'Connor, K. J.; Burrows, C. J. *J. Am. Chem. Soc.* **1990**, *112*, 4568–4570. (b) Ferreira, R.; García, H.; de Castro, B.; Freire, C. *Eur. J. Inorg. Chem.* **2005**, 4272–4279.

(42) Chatterjee, D.; Mukherjee, S.; Mitra, A. *J. Mol. Catal. A: Chem.* **2000**, *154*, 5–8.